Inorganic Chemistry

Open Access

pubs.acs.org/IC

Article

Elucidating the Non-Covalent Interactions that Trigger Interdigitation in Lead-Halide Layered Hybrid Perovskites

Arthur Maufort, Jesús Cerdá, Kristof Van Hecke, Davy Deduytsche, Arne Verding, Bart Ruttens, Wei Li, Christophe Detavernier, Laurence Lutsen, Claudio Quarti, Dirk Vanderzande, David Beljonne, and Wouter T. M. Van Gompel*

Cite This: *Inorg. Chem.* 2024, 63, 5568−5579

Read Online

ACCESS | Metrics & More | Article Recommendations | Supporting Information

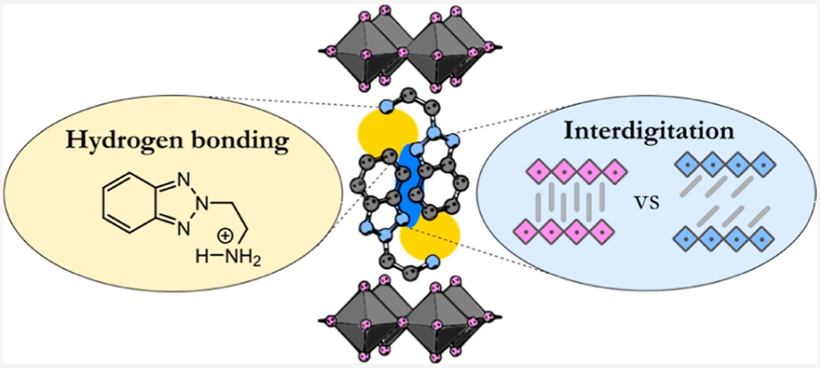

ABSTRACT: Two-dimensional (2D) hybrid organic−inorganic perovskites constitute a versatile class of materials applied to a variety of optoelectronic devices. These materials are composed of alternating layers of inorganic lead halide octahedra and organic ammonium cations. Most perovskite research studies so far have focused on organic sublattices based on phenethylammonium and alkylammonium cations, which are packed by van der Waals cohesive forces. Here, we report a more complex organic sublattice containing benzotriazole-based ammonium cations packed through interdigitated $\pi-\pi$ stacking and hydrogen bonding. Single crystals and thin films of four perovskite derivatives are studied in depth with optical spectroscopy and X-ray diffraction, supported by density-functional theory calculations. We quantify the lattice stabilization of interdigitation, dipole−dipole interactions, and inter- as well as intramolecular hydrogen bonding. Furthermore, we investigate the driving force behind interdigitation by defining a steric occupancy factor σ and tuning the composition of the organic and inorganic sublattice. We relate the phenomenon of interdigitation to the available lattice space and to weakened hydrogen bonding to the inorganic octahedra. Finally, we find that the stabilizing interactions in the organic sublattice slightly improve the thermal stability of the perovskite. This work sheds light on the design rules and structure−property relationships of 2D layered hybrid perovskites.

1. INTRODUCTION

Extensive research in the past decade has shown that solar cells based on hybrid organic−inorganic perovskites (HOIPs) might become a cornerstone in the future global energy economy.[1,2] Although three-dimensional (3D) HOIPs have been receiving a lot of attention, also their two-dimensional (2D) counterparts generate growing interest.[3−5] 3D and 2D HOIPs are based on the same metal halide salts but differ in the type of organic ammonium cations that are employed. Small organic cations such as methylammonium and formamidinium fit well in the cuboctahedral cavities, not interrupting the corner-shared connectivity of the metal halide octahedra in the perovskite motif. Above a certain size threshold, however, larger cations induce a separate self-assembly of alternating arrays of organic cations and inorganic sheets.[6,7] This alternative stacking results in distinct optoelectronic properties and potential applications for 2D HOIPs compared to their 3D analogues. Whereas the latter compete with the best contenders in solar cell[8] and photodetector[9,10] research, the former have favorable optoelectronic properties to produce performant light-emitting diodes (LEDs),[11,12] lasers,[13] transistors,[14] and passivating layers in perovskite-based solar cells.[3,15]

In these applications, hybrid perovskites are often applied as thin films. However, research into perovskite single crystals is

Received: December 21, 2023
Revised: February 13, 2024
Accepted: February 20, 2024
Published: March 12, 2024

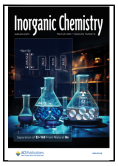

ACS Publications

https://doi.org/10.1021/acs.inorgchem.3c04536

also of high relevance since it can consolidate observations made for thin films whose polycrystalline nature generally complicates the determination of intrinsic material properties. Despite the rapid progress in research on single crystals of 3D HOIPs,[16,17] the amount of studies related to single crystals of 2D HOIPs remains comparatively limited, with the notable exception of 2D HOIPs containing phenethylammonium- and alkylammonium-based cations.[18−20] However, recent reports have shown that extended aromatic systems can improve the efficiency and/or stability in thin-film devices.[21] For example, carefully designed organic cations based on carbazole,[22−25] pyrene,[26] oligothiophene,[27−29] or benzothienobenzothiophene[30] have resulted in perovskite thin films with specific optoelectronic properties, such as improved charge carrier mobility[23,26,28] and lifetime.[23,24] Moreover, our research group[31−33] and others[34] have demonstrated the self-assembly of organic charge−transfer complexes into the organic layers of perovskite films by intercalating an acceptor chromophore into an organic layer containing electron donating organic cations, resulting in long-lived charge carriers[31] and a reduced exciton binding energy.[34] 2D HOIP single-crystal research with tailored aromatic moieties can therefore catalyze studies to ultimately maximize the figures of merit of various optoelectronic devices. However, for this to happen, it is crucial to gain insights into structure−property relationships and design rules of these advanced 2D HOIPs, which feature various non-covalent interactions.

Here, we provide an in-depth characterization of the atomic structures of thin films and single crystals of four benzotriazole-based 2D HOIPs. Recent work by some of the authors demonstrated that these 2D HOIPs can successfully be applied as interlayers in formamidinium lead iodide solar cells, improving the power conversion efficiency from 20% to nearly 22%.[35] Single-crystal analysis revealed that benzotriazole-based organic layers in lead(II) iodide lattices show interdigitation, reducing the thickness of the organic layer and leading to unusually dense aromatic packing. Moreover, 2D layered benzotriazole perovskites contain hydrogen bonds—both inter- and intramolecular—within the organic layers. Due to this hydrogen bonding pattern in the organic layer for the lead(ii) iodide perovskites, a negative penetration depth for the ammonium headgroup into the inorganic framework is obtained. This negative penetration depth is accompanied by a very small degree of octahedral tilting in the inorganic framework. Through theoretical density-functional theory (DFT) modeling, we elucidate these phenomena, disentangling the contributions from the various non-covalent interactions. In addition, we introduce an occupancy factor, σ, which may serve as a numerical descriptor to predict and rationalize the potential incorporation of bulky spacers and their packing in 2D halide perovskite lattices. It is shown that hydrogen bonds strengthen the interactions within the organic layers, ultimately templating inorganic layer crystallization and slightly enhancing thermal stability with respect to a literature reference 2D halide perovskite. This work improves the understanding of the complex interplay between lattice strain, non-covalent interactions, and thermal properties of 2D layered perovskites.

2. EXPERIMENTAL SECTION

2.1. Synthesis of Organic Cations. Detailed synthesis procedures are outlined and are illustrated in the Supporting Information.

2.2. Thin-Film Deposition. Precursor solutions for thin-film synthesis were prepared by dissolving stoichiometric amounts of the corresponding lead halide and organic halide in a mixture of dry *N*,*N*-dimethylformamide (DMF) and dry *N*,*N*-dimethylacetamide (DMAc). The amounts are included in the Supporting Information. The precursor elements were dissolved together at 50 °C and the resulting solutions were filtered through a syringe filter (0.2 μm pore size). The precursor solutions were spin coated on top of quartz substrates, which had been sonicated in dimethyl sulfoxide, deionized water, acetone, and isopropanol (15 min each) and had been treated by UV/ozone for 15 min prior to deposition. Spin coating and subsequent hot plate annealing were performed inside a nitrogen-filled glovebox (<1 ppm of O_2, <1 ppm of H_2O). Reference thin-films containing only the organic halide were spin-coated by omitting the lead halide in the precursor and by drying the films on a hot plate at 80 °C after spin coating. The perovskite thin films and the reference films were stored inside a nitrogen-filled glovebox and were removed only for analysis.

2.3. Single Crystal Growth. Perovskite single crystals were grown following the solvent conversion-induced crystallization method reported by Fateev et al.[36] Stoichiometric amounts of the organic halide and lead halide were dissolved in a mixture of propylene carbonate (PC), water, and HBr or HI (48% respectively 57% in water). HI was extracted three times with a 9:1 (v/v) mixture of chloroform and tri-*n*-butyl phosphate before use. Lead bromide-based mixtures were stirred at 40 °C and lead iodide-based mixtures were stirred at 50 °C until a clear solution was obtained. The solutions were then filtered through a syringe filter into a base-bath cleaned glass vial and were heated to their crystallization temperature. The lid of the vial was perforated with a needle to enable CO_2 to escape during the solvent degradation process. The exact precursor concentration, solvent mixture, and crystallization temperature used for each perovskite are summarized in the Supporting Information. $(BTa)_2PbBr_4$ and $(F_2BTa)_2PbBr_4$ crystallized as colorless platelets (37 and 24% yield, respectively); $(BTa)_2PbI_4$ and $(F_2BTa)_2PbI_4$ crystallized as orange needles (55 and 64% yield, respectively). Single-crystals of the BTaBr, BTaI, and F_2BTaI halide salts were grown through recrystallization from isopropanol.

2.4. Characterization. UV−vis−NIR absorption spectra were recorded on a Cary 5000 UV−vis−NIR spectrophotometer from Agilent Technologies. A cleaned quartz substrate was used as the calibration background. Photoluminescence (PL) emission spectra were recorded on a Horiba-Jobin Yvon Fluorolog-3 spectrofluorometer equipped with double-grating excitation and emission monochromators and a 450 W Xe lamp as a light source. The samples were excited at either 300 or 430 nm, which is specified in the relevant figure captions. X-ray diffraction (XRD) measurements were measured at ambient temperature and pressure on a Bruker D8 Discover diffractometer with CuK_α radiation. X-ray intensity data of single crystals were collected at 100 K on a Rigaku Oxford Diffraction Supernova Dual Source (Cu at zero) diffractometer equipped with an Atlas CCD detector using ω scans and CuK_α (λ = 1.54184 Å) radiation. Data processing is outlined in the Supporting Information. In situ XRD measurements were carried out on a Bruker D8 Discover XRD system equipped with a Cu X-ray source (λ = 1.5406 Å) and a linear X-ray detector. The samples were placed on a sample heating stage inside a closed annealing chamber. The XRD measurements were carried out under a N_2 atmosphere with a continuous nitrogen flow rate of 500 sccm at atmospheric pressure. Samples were heated via a stepwise temperature profile from RT up to 290 °C in steps of 5 °C. The temperature was measured with a K-type thermocouple. Every 5 °C, the temperature was stabilized for several seconds before an XRD scan from 2θ = 3 to 35° was taken at that specific temperature.

2.5. Computational Details. Computational details can be found in the Supporting Information.

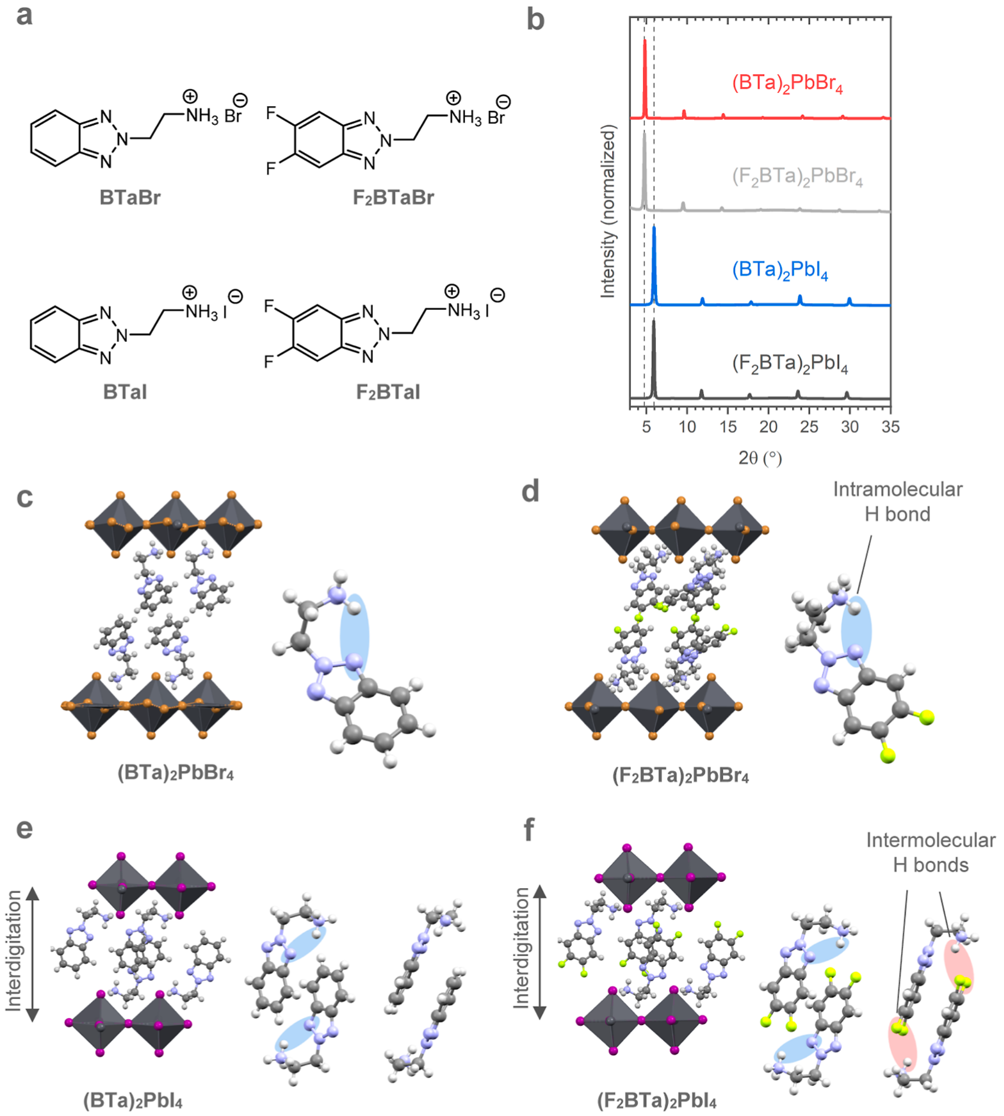

Figure 1. (a) Chemical structures of four benzotriazole-based ammonium salts and (b) thin-film XRD patterns of their corresponding lead(II) halide perovskites, displaying the characteristic (00*l*) reflections with l = 2, 4, 6... (c−f) Single-crystal X-ray structures of these perovskites, including a detailed conformation of the organic cations. Element color coding: gray (carbon), white (hydrogen), blue (nitrogen), yellow (fluorine), black (lead), brown (bromine), and purple (iodine).

3. RESULTS AND DISCUSSION

3.1. Synthesis and Structural Characterization of Benzotriazole Salts, Perovskite Thin Films, and Perovskite Single Crystals. In a previous study,[35] we have reported four benzotriazole-based ammonium salts, synthesized through a three-step reaction pathway comprising core formation, alkylation, and salt formation (Figure 1a and Scheme S1). This reaction sequence is designed to widen derivatization and extend the possibilities related to molecular design. Besides the pristine benzotriazole-based bromide salt (BTaBr) and iodide salt (BTaI), their respective difluorinated derivatives F_2BTaBr and F_2BTaI were also successfully obtained. Furthermore, to address the potential structural role of the spacer length, we also synthesized a derivative with a three-carbon spacer attached to the benzotriazole core to compare it with the two-carbon spacer (vide infra). Finally, another advantage of the chosen reaction sequence is that it incorporates the synthesis of *tert*-butyloxycarbonyl (Boc)-protected amines, which are generally easier to handle and purify than their unprotected amine counterparts. Therefore, this three-step pathway can efficiently generate various benzotriazole-based ammonium salts.

The four benzotriazole-based ammonium salts BTaBr, F_2BTaBr, BTaI, and F_2BTaI were subsequently incorporated into 2D layered perovskite single crystals and thin films. Thin films were deposited through spin coating precursor solutions of the corresponding ammonium salt and lead(II) halide salt in a 2:1 molar ratio, followed by hot plate annealing (see the Supporting Information). The XRD patterns of these thin films are depicted in Figure 1b. The corresponding UV−vis absorption and photoluminescence (PL) emission spectra are reported in Figure S1. The XRD patterns show the typical (00*l*) reflections with *l* = 2, 4, 6... characteristic for 2D HOIP thin films with preferential growth of the inorganic sheets parallel to the substrate.[37] Interestingly, the first-order reflection of the iodide perovskites appears at a markedly higher angle than that of the first-order reflection of the bromide perovskites. Through Bragg's law, the calculated interplanar distance (d_{00l}) amounts to 18.4 and 18.7 Å for

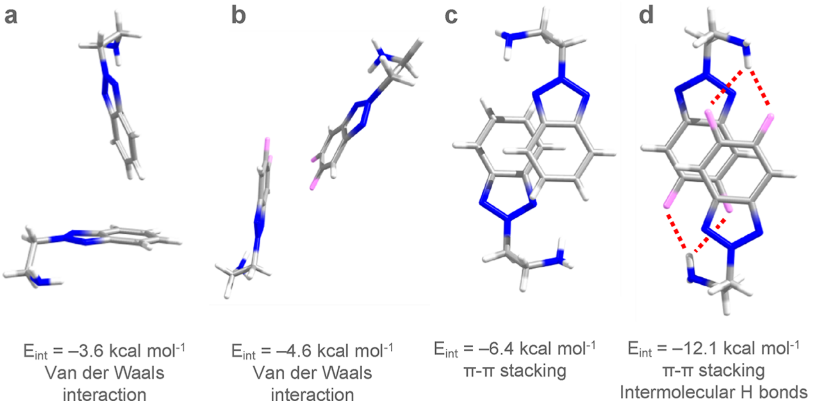

Figure 2. Most compact organic dimers extracted from the X-ray structures of (a) $(BTa)_2PbBr_4$, (b) $(F_2BTa)_2PbBr_4$, (c) $(BTa)_2PbI_4$, and (d) $(F_2BTa)_2PbI_4$ together with the corresponding interaction energies. The ammonium groups were substituted by amine groups to ensure charge neutrality.

$(BTa)_2PbBr_4$ and $(F_2BTa)_2PbBr_4$, respectively, whereas the interplanar distance amounts to only 14.9 and 15.0 Å for $(BTa)_2PbI_4$ and $(F_2BTa)_2PbI_4$, respectively. This significant interplanar shrinkage of 3.5 and 3.7 Å when replacing bromide by iodide is rather large compared to the literature.[37,38] For example, a similar halide substitution in widely investigated phenylethylammonium- and butylammonium-based perovskites leads to a compression of the interlayer distance of only 1.1 and 0.7 Å, respectively.[18,37,39] The corresponding crystal structures, determined via single-crystal XRD, are depicted in Figure 1c−f, of which the simulated powder XRD patterns show the same trend as the corresponding thin-film XRD patterns (Figure S2). The detailed procedure for single-crystal synthesis and characterization is reported in the Supporting Information. The interplanar shrinkage is explained by the peculiar packing of the benzotriazole cations in the iodide perovskites depicted in Figure 1d,f. Here, the aromatic cations anchored to adjacent inorganic layers interdigitate and form $\pi-\pi$ conjugated stacks along the crystallographic c axis (Figure S3). The concept of interdigitation is defined in Figure S4 and indicates that the two molecular stacks, of which each organic bilayer is composed, slide into each other like two hands with fingers intertwined. In contrast, the aromatic planes in the bromide perovskites do not interdigitate and form a more traditional bilayer of organic cations. This bilayer stacking is typical for state-of-the-art 2D HOIPs containing monoammonium organic cations, featuring a van der Waals gap with cohesive non-covalent forces. We anticipate that the interdigitated stacking results in stronger intermolecular interactions in the organic sublattice compared to classical 2D HOIPs with van der Waals gaps.

Interdigitating organic bilayers have been described in the literature for extended alkylammonium cations in 2D lead iodide-based lattices, while bromide-based lattices have not been studied in this context yet.[18,40] In these alkylammonium-based 2D HOIPs, only cohesive van der Waals forces act on the organic cations. It has been demonstrated that, if these alkyl tails become long enough, the organic layers are strongly held together, templating the crystal structure of the inorganic component.[41] However, the phenomenon of interdigitation has, to the best of our knowledge, not yet been observed in 2D HOIPs with aromatic organic cations.[26,37,38,42−44] Most noteworthy, the incorporation of benzotriazole-based organic spacers, as proposed here, greatly extends the range of non-covalent interactions from only van der Waals forces to aromatic $\pi-\pi$ interactions, dipole−dipole interactions, and hydrogen bonds. Since the occurrence of interdigitation in the organic layers of these benzotriazole perovskites can be tuned by the halide, this class of materials presents an ideal test bench to study in detail which of these forces drive interdigitation.

The single-crystal structures highlight the formation of hydrogen bonds in the organic sublattice for all four perovskite structures. In each benzotriazole cation, the ammonium headgroup points back to one of the nitrogen atoms of its own aromatic core, which acts as a hydrogen bond acceptor. This intramolecular hydrogen bonding gives rise to a seldomly encountered negative penetration depth in the iodide perovskites, whereby the ammonium group points out of the inorganic sheet.[37,45] So far, this has only been observed for 2D HOIPs featuring 2-haloalkylammonium cations, in which the ammonium headgroup forms a hydrogen bond with the halide substituent.[46−48] This negative penetration depth is accompanied by a very small octahedral tilting in the inorganic framework, which is in line with previous studies.[37,46] More specifically, the in-plane deviation from linearity of the Pb−I−Pb angle amounts to 6.6 and 4.7° for $(BTa)_2PbI_4$ and $(F_2BTa)_2PbI_4$, respectively, and the out-of-plane distortion is zero for both (Figure S5). In addition to intramolecular hydrogen bonding, $(F_2BTa)_2PbI_4$ (Figure 1f) also displays intermolecular hydrogen bonding. More specifically, the ammonium head groups here also interact with the two fluorine atoms of the neighboring molecule. This results in the occurrence of four non-covalent interactions within the organic layers in this compound: aromatic $\pi-\pi$ stacking, dipole−dipole interactions, and intra- as well as intermolecular hydrogen bonding. It is expected that the balance between these interactions is responsible for the occurrence of interdigitation in the organic layer.

3.2. First-Principles Calculations of Intra- and Intermolecular Interactions.

With the aim to understand the interplay between non-covalent interactions in the lattice, the size constraints imposed by the lead-halide framework, and the observed interdigitation, we resorted to DFT electronic structure calculations.

First, we estimated the intramolecular hydrogen bond strength in $(BTa)_2PbI_4$ to be 14.2 kcal mol^{-1} through a rigid scan of the torsion angle of the ammonium group with respect to the aromatic core (Figure S6), performed at the B3LYP-D3/cc-pVTZ level of theory. This value is at the upper edge of what is expected for a hydrogen bond, likely because it involves a positively charged hydrogen bond donor. Actually, the intramolecular hydrogen bond strength in the non-charged benzotriazole amine unit is 4.0 kcal mol^{-1} (Figure S6). The intramolecular hydrogen bonds in the other derivatives in Figure 1c−f are expected to be similar in strength since the benzotriazole cation geometry in the four perovskite lattices is also similar.

Next, we estimated the interaction energy in the closest pairs of BTa molecules and F_2BTa molecules in their respective 2D HOIP single-crystal lattice (Figure 2). The interaction energy of a pair is defined as the total energy difference between the non-charged amine dimer and its two isolated composing molecules, all with the same geometry as in the crystal lattice. We opted for non-charged amine dimers to exclude Coulombic repulsion from the calculations. The resulting interaction energy amounts to −6.4 (−12.1) kcal mol^{-1} for the BTa (F_2BTa) dimer in the PbI_2-based lattice and reduces to −3.6 (−4.6) kcal mol^{-1} in the $PbBr_2$-based lattice. The interaction energy is the largest in $(F_2BTa)_2PbI_4$, with four intermolecular H···F hydrogen bonds contributing an energy stabilization of 5.7 kcal mol^{-1} compared to that in $(BTa)_2PbI_4$, which does not feature such hydrogen bonds. Thus, we estimate a single intermolecular hydrogen bond strength of about 1.4 kcal mol^{-1} in the F_2BTa dimer. This value is smaller than in other hydrogen-bond driven crystals or molecular stacks, which is in accordance with the relatively large N−H···F distances of 2.47 and 2.72 Å.[49−51]

We then analyzed the aromatic $\pi-\pi$ and dipole−dipole contributions to the interaction energies in the iodide perovskites (Figure 1e,f). For this purpose, we substituted the alkylammonium tails with hydrogen atoms and performed a 2D scan of the interaction energy by slipping one of the BTa (F_2BTa) cores in the molecular plane while keeping the interplanar distance to its equilibrium value. The heatmaps in Figure S7 show that the arrangement found in the perovskite crystal structure corresponds to the largest interaction energy (most stable arrangement), both for BTa and F_2BTa. Figure S7 also suggests that a displacement of (−3 Å, 2 Å) along the (x, y) axis leads to a repulsive interaction in the F_2BTa dimer, while this is not the case for the BTa dimer. From Figure S7, similar contributions are calculated in the BTa and F_2BTa dimer (−6.0 and −6.4 kcal mol^{-1}, respectively), which stem from $\pi-\pi$ and dipole−dipole interactions. Notably, this interaction energy, which excludes the hydrogen bond component, is nearly the same in the BTa and the F_2BTa dimer, in spite of the substantially larger dipole moment of the latter (0.75 and 3.22 D, respectively). This suggests that dipole−dipole interactions are not dominant in the present case, likely because of the short distance between the aromatic planes. We close this analysis stressing the much smaller intermolecular interaction energies in the bromide perovskites (−3.6 kcal mol^{-1} for BTa and −4.6 kcal mol^{-1} for F_2BTa). In this case, the larger distance between the aromatic cores and their relative orientation precludes the formation of effective intermolecular hydrogen bonds and $\pi-\pi$ interactions (Figure 2). Note again that the interaction energies in the F_2BTa pairs are larger than those in the corresponding BTa pairs.

We now move to clarify why the interdigitated packing of the organic aromatic planes occurs only in the iodide perovskites. The simplest explanation is related to steric effects, i.e., the fact that the larger Pb−I lattice provides sufficient space for interdigitation, while the smaller Pb−Br lattice does not. Figure 3 compares the 2D perovskite framework of $(F_2BTa)_2PbBr_4$ and $(F_2BTa)_2PbI_4$, highlighting a 20% increase in the surface that hosts the organic cation on going from a bromide to an iodide lattice. Notice also that, as already mentioned earlier, the iodide lattice features almost zero octahedral tilting (Pb−I−Pb angles of 175.3 and 177.9°, Figure S5), hence maximizing the surface area of the octahedral cavity. Octahedral tilting in 2D HOIPs is a well-known mechanism for the release of mechanical stress associated with lattice strain between the inorganic frame and the spacer.[52] Inspired by the ionic fill factor proposed by Sato and co-workers,[53] we further defined a Goldschmidt-like occupancy factor for 2D-layered perovskites. More specifically, we estimated the volume available to host the organic cation starting from the surface available per Pb atom in Figure 3 and from the height of the organic cation (Figure S8). Subsequently, we divided this volume by the volume of the organic cation (Figure S8). The resulting occupancy factors of σ amount to 2.03 and 1.42 cations per Pb atom for $(F_2BTa)_2PbI_4$ and $(F_2BTa)_2PbBr_4$, respectively. Though approximate, this simple calculation clearly indicates that the iodide-based lattice presents sufficient space to accommodate two benzotriazole units, hence allowing interdigitation, while this is not the case for the bromide lattice.

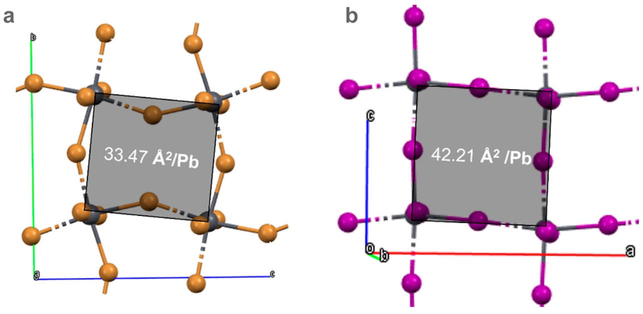

Figure 3. Top view of the inorganic lattice of (a) $(F_2BTa)_2PbBr_4$ and (b) $(F_2BTa)_2PbI_4$. The shadowed zones display the measured transversal area.

We complement this steric argument with an energetic one. Starting from the experimental single-crystal structures, we designed alternative crystal models in which $(F_2BTa)_2PbBr_4$ presents the same interdigitated packing as $(F_2BTa)_2PbI_4$, and vice versa. We then optimized these periodic structures using plane-wave simulations along with the van der Waals corrected vdw-df2 functional including non-local dispersion corrections.[54,55] The resulting structures are illustrated in Figure S9. After optimization, the native structures were found to be more stable than the alternative structures by 0.6 kcal mol^{-1} per chemical unit for $(F_2BTa)_2PbI_4$ and by 9.11 kcal mol^{-1} per chemical unit for $(F_2BTa)_2PbBr_4$. Interestingly, the energy penalty for the iodide perovskite to adopt a non-interdigitated packing, such as the one encountered in the bromide perovskite, is only moderate. In contrast, the energy penalty estimated for the bromide perovskite to adopt the interdigitated perovskite packing of the iodide perovskite amounts to almost 15 times the k_BT at room temperature. This finding harmonizes with the occupancy factor argument developed above.

We complete the analysis of organic cation packing in benzotriazole perovskites by estimating the energy (E_{int}) needed to separate two consecutive inorganic layers, along with their anchored benzotriazole cations, by 100 Å (Figure S10). We estimated E_{int} for the native and hypothetical alternative crystal structures of $(F_2BTa)_2PbI_4$ and $(F_2BTa)_2PbBr_4$. Table 1 displays the estimated interaction energies and shows that both non-interdigitated packings, i.e., the native packing of the bromide perovskite and the alternative packing of the iodide perovskite, present a similar interaction energy of about 0.70 kcal mol^{-1} per chemical unit. This is expected since the interaction energy of two adjacent organic layers mainly arises from the Van de Waals gap in between them, which mainly depends on the organic cations and not on the halides. On the other hand, the computed interaction energy amounts to 1.85 kcal mol^{-1} in the interdigitated packing of the iodide perovskite, but only to 0.08 kcal mol^{-1} per chemical unit in the interdigitated packing of the bromide perovskite. Hence, interdigitation stabilizes $(F_2BTa)_2PbI_4$ with respect to its hypothetical non-interdigitated packing ($\Delta E = -1.1$ kcal mol^{-1}). Instead, interdigitation is detrimental to $(F_2BTa)_2PbBr_4$ and leads to a significant increase of the interaction energy between the organic layers ($\Delta E = +0.60$ kcal mol^{-1}), which adversely affects the crystal cohesion energy.[56]

Table 1. Interaction Energy (E_{int}) in kcal mol^{-1} per Chemical Unit Estimated for the Interdigitated and Non-Interdigitated Packings of $(F_2BTa)_2PbI_4$ and $(F_2BTa)_2PbBr_4$ in Figure S10

E_{int} (kcal mol^{-1})	$(F_2BTa)_2PbBr_4$	$(F_2BTa)_2PbI_4$
Interdigitated packing	0.08	1.85
Non-interdigitated packing	0.68	0.75

3.3. Derivatives of Benzotriazole Perovskites.

Having established and quantified interdigitation, hydrogen bonding, $\pi-\pi$ interactions, and dipole−dipole interactions in the four benzotriazole perovskites from Figure 1c−f, we proceeded by altering the composition of this class of perovskites to fully grasp the fundamental driving force behind interdigitation in benzotriazole perovskites. To accomplish this, we investigated three derived systems: (i) mixed-halide thin films in which iodide is gradually substituted by bromide, to elaborate on the effect of lattice strain on interdigitation through halide substitution; (ii) PbI_2-based thin films containing a benzotriazole-based ammonium salt with a three-carbon alkyl spacer instead of a two-carbon one, which we hypothesized would disfavor intramolecular hydrogen bonding; and (iii) single crystals of the organic ammonium salts outside a perovskite lattice, so without the presence of lead(II) halides in order to compare the packing of the organic cations inside and outside the inorganic lattice.

3.3.1. Mixed-Halide Thin Films.

In the previous section, we established that a certain minimum lattice space is required to provide the organic cations with the molecular degrees of freedom required to interdigitate. To study this phenomenon in further detail, mixed-halide perovskites were deposited. Stoichiometric precursor solutions of benzotriazole-based mixed halide perovskites were spin-coated and annealed at an optimal temperature of 125 °C, which is between the annealing temperature of pure iodide thin films (120 °C) and pure bromide thin films (130 °C). The XRD patterns of these mixed halide perovskites are depicted in Figure 4a; the corresponding UV−vis absorption spectra are given in Figure S11. The XRD patterns show that, at least until 30% mixing, bromide can substitute iodide in $(BTa)_2PbI_4$ while preserving interdigitation, as can also be seen from the interplanar distance d_{00l} (Figure 4b). In a similar way, iodide can partially substitute for bromide in $(BTa)_2PbBr_4$ without causing interdigitation. In the corresponding absorption spectra, the excitonic peak of the pure bromide film gradually shifts from 395 to 408 nm as iodide gets incorporated. Likewise, the excitonic peak of the pure iodide film gradually shifts from 523 to 497 nm upon bromide incorporation (Figure S12). Beyond these final peak wavelengths, phase separation occurs, which is also apparent in the XRD pattern of $(BTa)_2Pb(Br_{0.5}I_{0.5})_4$ in Figure 4a. This means that no intermediate structure exists: the benzotriazole molecules pack either in an interdigitated layer motif or in a classical bilayer one. If the halide mix in the precursor does not match with the lattice requirements to form an interdigitated packing only nor with a bilayer packing only, a mixture of both phases will be formed. This is in contrast with some examples in the literature, where mixed-halide 2D perovskite systems exist that are miscible at all halide ratios (Figure S12).[38] It, again, indicates that interdigitation stabilizes the perovskite lattice: if too many bromide anions are present in the iodide precursor, an iodide-rich phase with interdigitation in the organic layer perseveres to exist and the remaining

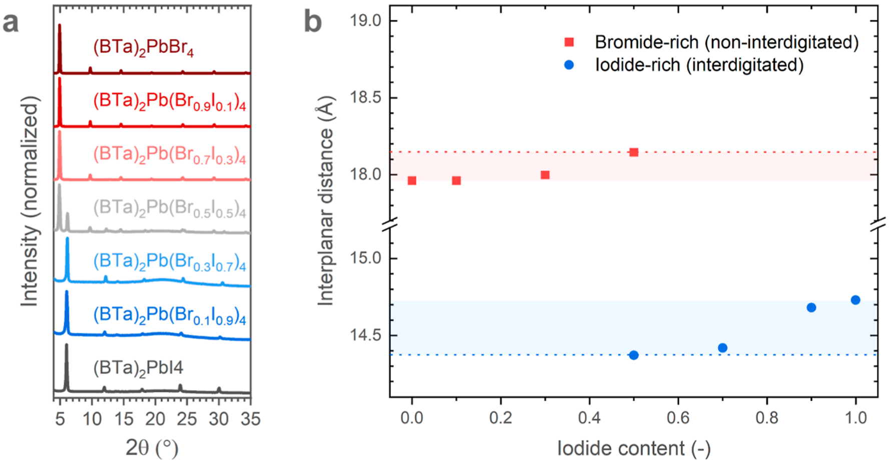

Figure 4. (a) Thin-film XRD patterns of mixed halide perovskites featuring the BTa cation. All films were annealed at 125 °C. (b) Shift of the interplanar distance as a function of the iodide content. The interplanar distance was derived from the first-order reflection of the corresponding XRD patterns through Bragg's law. The dotted lines are guides to the eye.

bromide-rich precursor part forms a separate non-interdigitated phase.

3.3.2. Perovskite Thin Films Containing a Benzotriazole Derivative with a Three-Carbon Alkyl Spacer.

We synthesized a benzotriazole derivative with a three-carbon spacer (Figure 5) through the same synthesis route that yielded the other four ammonium salts in Figure 1a. We hypothesized that, by increasing the spacer length from two to three carbons, intramolecular hydrogen bonding in the organic cation should be discouraged in favor of hydrogen bonding to the inorganic lattice, as a six-membered ring configuration would have to be substituted by a less favorable seven-membered ring configuration to accommodate the intramolecular hydrogen bond (Figure S13).[57,58] To verify this hypothesis, we spin-coated stoichiometric precursor solutions containing this modified benzotriazole cation and lead(II) iodide, followed by hot plate annealing. UV−vis absorption and PL emission spectra are included in Figure S14, in which the hot plate annealing temperature was varied to observe potential changes in the crystal phase as a function of temperature. The excitonic absorption and emission peak appear in the wavelength region of 490 nm for all relevant temperatures (100 °C until 140 °C), indicating that this modified benzotriazole cation also forms a 2D perovskite. With a peak value of ∼490 nm, the excitonic absorption peak for this 2D perovskite is located at a notably lower wavelength value than the excitonic absorption peak of $(BTa)_2PbI_4$ (523 nm) and $(F_2BTa)_2PbI_4$ (527 nm) (Figure S1). Given the known relationship between octahedral tilting and excitonic peak value,[59] this shift to a lower wavelength implies that the octahedral tilting is significantly larger in this perovskite. A higher degree of octahedral tilting likely stems from a deeper penetration of the ammonium headgroup into the inorganic plane, which points to stronger hydrogen bonding of the ammonium group to the inorganic lattice.[37] This tentatively confirms our hypothesis that intramolecular hydrogen bonding should become weaker due to the extension of the spacer from two to three carbons.

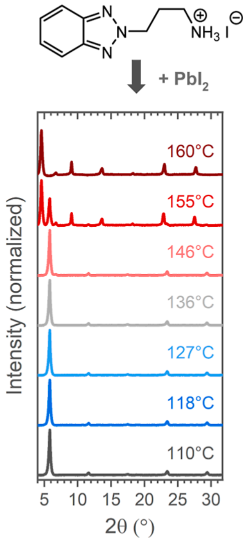

Figure 5. Thin-film XRD series of perovskite thin films featuring a benzotriazole-based cation with a three-carbon spacer during in situ heating from 110 to 160 °C. The film was preannealed at 110 °C.

Additionally, Figure 5 shows an XRD measurement with in situ heating from 110 to 160 °C, performed on a film which was preannealed at 110 °C to form the 2D perovskite phase and which was subsequently cooled to ambient temperature. Strikingly, a phase transition is observed, which also appears in an experiment with varied annealing temperature on a hot plate (Figure S15). Whereas the first-order reflection appears at 5.8° 2*θ* at 110 °C in Figure 5, this phase has completely disappeared at 160 °C, and a new phase with a first-order reflection at 4.6° 2*θ* appears instead, together with a small reflection corresponding to an impurity phase at 6.7° 2*θ*. Through Bragg's law, these reflections translate into an interplanar distance of 15.2 Å for the low-temperature phase and 19.4 Å for the high-temperature phase. The great similarity with the XRD patterns in Figures 1b and 4a strongly suggests that the low-temperature phase contains an interdigitated organic layer and that the high-temperature phase contains a non-interdigitated organic bilayer. Although this transition from an interdigitated phase to a non-interdigitated phase is observed as temperature increases, the opposite is not observed: upon cooling the non-interdigitated phase back to ambient temperature, the interdigitated phase is not regenerated. This phase transition therefore seems to be irreversible, with a certain energy barrier that must be overcome. We hypothesize that the expectedly weaker intramolecular hydrogen bonding in the modified benzotriazole cation changes the balance of forces such that both an interdigitated and a non-interdigitated 2D perovskite phase can form. The weakened intramolecular hydrogen bond likely results in a stronger interaction of the ammonium group with the inorganic octahedra, affecting the octahedral tilting and, in that way, the steric occupancy factor of this 2D perovskite.

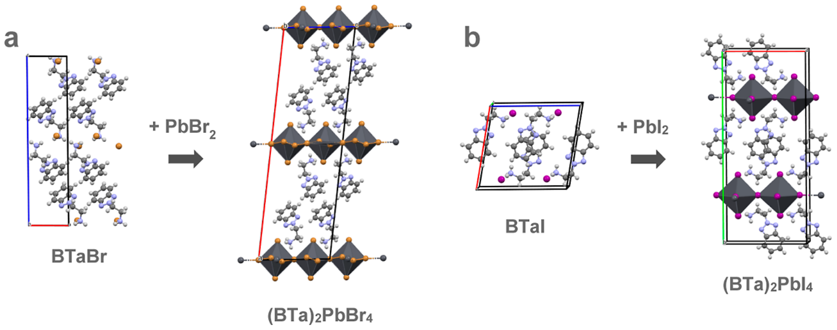

Figure 6. Single crystal X-ray structure comparison between the organic reference salts (a) BTaBr and (b) BTaI and their corresponding lead(II) halide perovskite. The same element color codes apply as those in Figure 1.

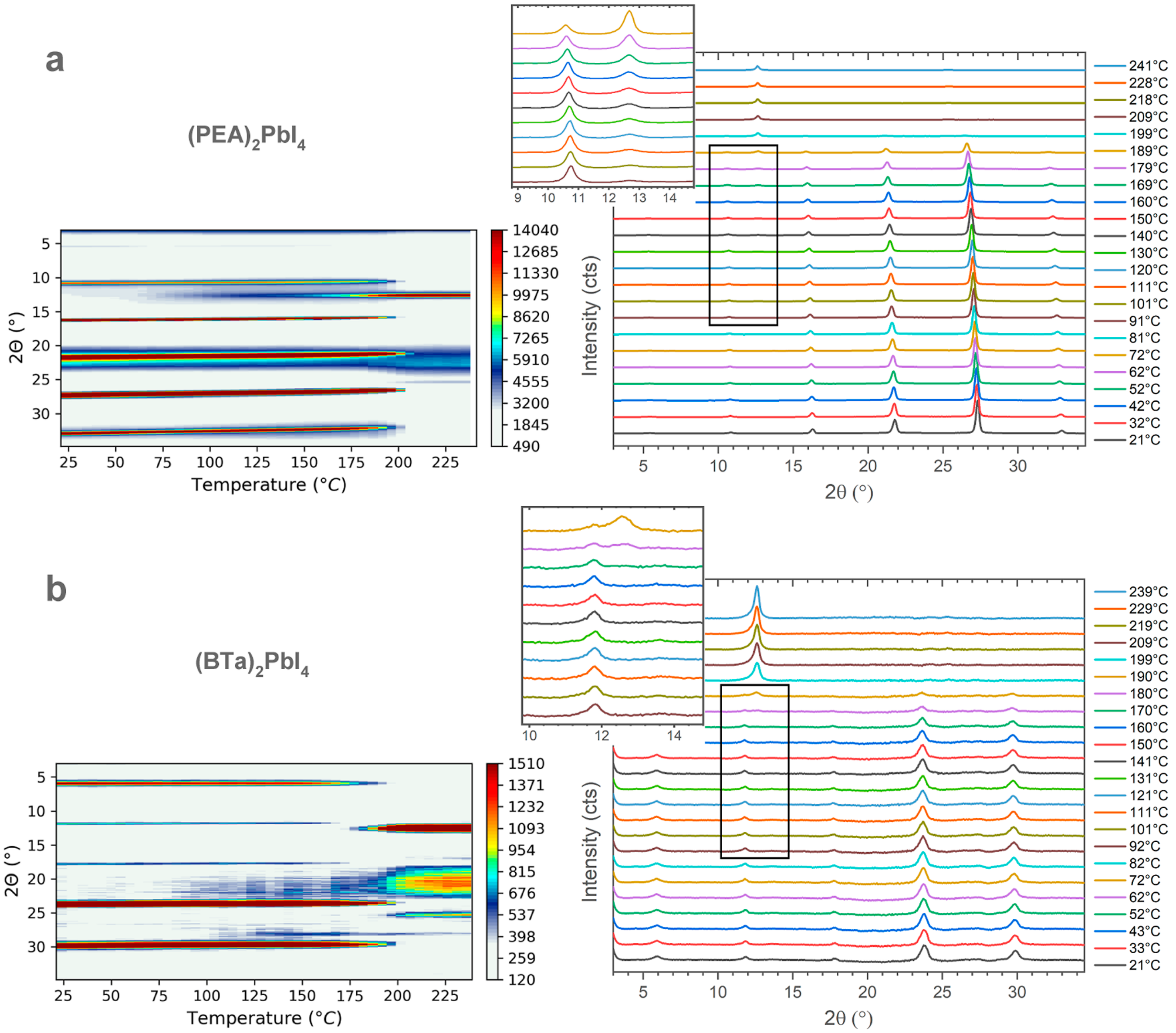

Figure 7. Thin-film XRD measurements with in situ heating on (a) (PEA)$_2$PbI$_4$ and (b) (BTa)$_2$PbI$_4$.

3.3.3. Organic Cation Reference Single Crystals. We further elucidate the interplay between intramolecular hydrogen bonding and interdigitation by growing single crystals of the BTaI, F$_2$BTaI, and BTaBr ammonium salts in the absence of lead halide salts to compare the arrangement of the organic layers inside and outside of the perovskite lattice. All of these reference crystals could be grown through recrystallization from isopropyl alcohol. The resulting crystal structures are displayed in Figures 6 and S16. In all three cases, the organic layer packing within and without the perovskite lattice is surprisingly similar. This is especially remarkable in the case of BTaBr, which retains its non-interdigitated packing despite the absence of the strain imposed by the lead-bromide perovskite lattice. Compared with BTaI, the only difference is the nature of the halide, leading to a completely different arrangement of the benzotriazole aromatic cores. BTaI and BTaBr are expected to differ in the strength of the interaction between the ammonium headgroup and the halide anion. The isolated bromide anion in particular should be a better hydrogen bond acceptor than the isolated iodide anion, and therefore, it is reasonable to assume that hydrogen bonding with the halide anion in the BTaBr salt is stronger than in the BTaI salt.[60] In other words, going from BTaBr to BTaI, ammonium-halide hydrogen bonding becomes weaker, and in turn, intramolecular hydrogen bonding and interdigitation emerge. It therefore seems that, in a 2D perovskite lattice with BTaBr, BTaI, and F$_2$BTaI, two conditions need to be met to observe interdigitation: (i) there should be sufficient space available as estimated via the steric occupancy factor σ (Figures 3 and S8), which should be larger than 2, and (ii) the hydrogen bonding between the ammonium headgroup and the inorganic lattice has to be relatively weak, to favor organic−organic interactions.

3.4. Consequences of Hydrogen Bonding and Interdigitation: Thermal Stability.

Finally, we investigated the effect of hydrogen bonding and interdigitated $\pi-\pi$ stacking in the organic layers on the thermal stability of the 2D layered perovskites. The thermal stability was benchmarked against the phenylethylammonium (PEA)-based perovskite (PEA)$_2$PbI$_4$, which also contains aromatic cations but does not feature inter- or intramolecular hydrogen bonding or interdigitated stacking within the organic layers. In this sense, $(PEA)_2PbI_4$ presents a classical van der Waals gap between adjacent layers of organic spacers.

We conducted XRD measurements on thin films with in situ heating from ambient temperature to 240 °C under an inert atmosphere (Figures 7 and S17). In these figures, the same (00*l*) reflections with *l* = 0, 2, 4, 6... as in Figure 1b are apparent at ambient temperature, which transition into the characteristic reflections of lead(II) iodide at $2\theta = 12.7$ and 25.5° when the temperature exceeds the thermal stability limit. Although both the PEA and benzotriazole perovskite reflections disappear at a similar temperature of 190 °C, indicating complete decomposition of the perovskite structure, the PbI_2 reflection at 12.7° already starts showing up at 100 °C in the PEA perovskite sample. This suggests that the PEA perovskite already starts to degrade partially at 100 °C, in contrast to the benzotriazole sample. The interdigitated benzotriazole layers therefore suppress the partial degradation of the perovskite into PbI_2, hence slightly improving the phase stability.

Although benzotriazole perovskites contain hydrogen bonds and interdigitated $\pi-\pi$ stacking in their organic layers, the thin-film thermal stability is only moderately improved. In contrast, earlier work by some of the authors has shown that, for example, the incorporation of a rigid benzothieno[3,2-*b*]benzothiophene (BTBT) cation resulted in a perovskite thermal stability improvement from 180 to 270 °C in a cesium lead iodide-based multilayered perovskite film with respect to the equivalent butylammonium perovskite.[30] In contrast to the BTBT-based 2D perovskite, the additional interactions in the benzotriazole-based organic layers only slightly improve the perovskite thermal stability. We hypothesize that the moderate increase in thermal stability in the benzotriazole perovskites with respect to the PEA reference could be related to the low octahedral tilting in the inorganic layers in the former, which is known to impose mechanical stress on the inorganic perovskite framework.[52] This increase in mechanical stress by the linearization of the inorganic framework may partly counteract the expected increase in stability due to stronger non-covalent interactions in the organic layers.

4. CONCLUSIONS

In this work, we presented benzotriazole-based 2D layered perovskites as an easily accessible class of perovskite materials that give rise to various non-covalent interactions: intermolecular hydrogen bonding, intramolecular hydrogen bonding, $\pi-\pi$ stacking, and dipole−dipole interactions. Furthermore, we observed rare interdigitation of the benzotriazole cations in iodide perovskites. Through DFT modeling, we showed that this interdigitation stabilizes the hybrid perovskite lattice. We defined a steric occupancy factor σ to compare the volume of the spacer with the total volume available in the interlayer region to host this spacer. Combined with experimental results, the modeling confirms that interdigitation within a 2D perovskite lattice occurs if $\sigma > 2$, that is, if the space available is sufficient, and if hydrogen bonding between the ammonium head groups and the inorganic layers is significantly weakened. Through experiments with mixed-halide perovskites, we showed that the interdigitated packing in the organic layers of the iodide perovskites drives the crystallization of the inorganic layers. Finally, the thin-film thermal stability is slightly improved by suppressing the formation of PbI_2 with respect to a PEA-based benchmark. This work improves the general understanding of the complex interplay between lattice strain and various non-covalent interactions in determining the crystal structure and the thermal stability of 2D HOIPs. We expect that benzotriazole derivatives will serve as a versatile platform for further studies of the structure−property relationships and design rules of 2D HOIPs.

■ ASSOCIATED CONTENT

Supporting Information

The Supporting Information is available free of charge at https://pubs.acs.org/doi/10.1021/acs.inorgchem.3c04536.

> Experimental details of the organic synthesis, thin-film deposition, single-crystal synthesis, single-crystal data, computational details, absorption and emission spectra, thin-film XRD patterns, and in situ temperature-controlled XRD patterns (PDF)

Accession Codes

CCDC 2305941−2305943 contain the supplementary crystallographic data for this paper. These data can be obtained free of charge via www.ccdc.cam.ac.uk/data_request/cif, or by emailing data_request@ccdc.cam.ac.uk, or by contacting The Cambridge Crystallographic Data Centre, 12 Union Road, Cambridge CB2 1EZ, UK; fax: +44 1223 336033.

■ AUTHOR INFORMATION

Corresponding Author

Wouter T. M. Van Gompel − *Hybrid Materials Design, Institute for Materials Research (imo-imomec), Hasselt University, B-3500 Hasselt, Belgium;* orcid.org/0000-0002-8173-5206; Email: wouter.vangompel@uhasselt.be

Authors

Arthur Maufort − *Hybrid Materials Design, Institute for Materials Research (imo-imomec), Hasselt University, B-3500 Hasselt, Belgium;* orcid.org/0000-0001-9621-6014
Jesús Cerdá − *Laboratory for Chemistry of Novel Materials, University of Mons, B-7000 Mons, Belgium*
Kristof Van Hecke − *XStruct, Department of Chemistry, Ghent University, B-9000 Ghent, Belgium;* orcid.org/0000-0002-2455-8856
Davy Deduytsche − *Conformal Coating of Nanomaterials, Department of Solid State Sciences, Ghent University, B-9000 Ghent, Belgium*
Arne Verding − *Hybrid Materials Design, Institute for Materials Research (imo-imomec), Hasselt University, B-3500 Hasselt, Belgium*
Bart Ruttens − *Imec-imomec, B-3590 Diepenbeek, Belgium*
Wei Li − *Laboratory for Chemistry of Novel Materials, University of Mons, B-7000 Mons, Belgium;* Present Address: School of Chemistry and Material Science, Hunan Agricultural University, Nongda Road 1, 410128 Changsha, China; orcid.org/0000-0002-9999-5081
Christophe Detavernier − *Conformal Coating of Nanomaterials, Department of Solid State Sciences, Ghent University, B-9000 Ghent, Belgium*
Laurence Lutsen − *Hybrid Materials Design, Institute for Materials Research (imo-imomec), Hasselt University, B-3500 Hasselt, Belgium; Imec-imomec, B-3590 Diepenbeek, Belgium*
Claudio Quarti − *Laboratory for Chemistry of Novel Materials, University of Mons, B-7000 Mons, Belgium;* orcid.org/0000-0002-5488-1216

Dirk Vanderzande − *Hybrid Materials Design, Institute for Materials Research (imo-imomec), Hasselt University, B-3500 Hasselt, Belgium; Imec-imomec, B-3590 Diepenbeek, Belgium;* orcid.org/0000-0002-9110-124X

David Beljonne − *Laboratory for Chemistry of Novel Materials, University of Mons, B-7000 Mons, Belgium;* orcid.org/0000-0002-2989-3557

Complete contact information is available at:
https://pubs.acs.org/10.1021/acs.inorgchem.3c04536

Author Contributions

The manuscript was written through contributions of all authors. All authors have given approval to the final version of the manuscript.

Notes

The authors declare no competing financial interest.

■ ACKNOWLEDGMENTS

A.M. acknowledges the Research Foundation Flanders (FWO) for the funding of his FWO fundamental research PhD grant (1115721N). W.T.M.V.G., K.V.H., L.L., and D.V. acknowledge the FWO for the funding of the SBO project PROCEED (S002019N) and the senior FWO research projects G043320N and G0A8723N. K.V.H. also thanks the FWO for funding through project AUGE/11/029. Computational resources were provided by the Consortium des Équipements de Calcul Intensif (CÉCI) funded by the Belgian National Fund for Scientific Research (F.R.S.-FNRS) under Grant 2.5020.11. The present research also benefited from computational resources made available on Lucia, the Tier-1 supercomputer of the Walloon Region, infrastructure funded by the Walloon Region under the grant agreement no. 1910247. The work at the University of Mons was performed within the frame of the M-ERA.NET project PHANTASTIC (R.8003.22), supported by the FNRS. C.Q. is a FNRS research associate, and D.B. is a FNRS research director.

■ REFERENCES

(1) Liu, J.; De Bastiani, M.; Aydin, E.; Harrison, G. T.; Gao, Y.; Pradhan, R. R.; Eswaran, M. K.; Mandal, M.; Yan, W.; Seitkhan, A.; Babics, M.; Subbiah, A. S.; Ugur, E.; Xu, F.; Xu, L.; Wang, M.; Rehman, A. U.; Razzaq, A.; Kang, J.; Azmi, R.; Said, A. A.; Isikgor, F. H.; Allen, T. G.; Andrienko, D.; Schwingenschlögl, U.; Laquai, F.; De Wolf, S. Efficient and stable perovskite-silicon tandem solar cells through contact displacement by MgF_x. *Science* **2022**, *377* (6603), 302−306.

(2) Jiang, Q.; Tong, J.; Scheidt, R. A.; Wang, X.; Louks, A. E.; Xian, Y.; Tirawat, R.; Palmstrom, A. F.; Hautzinger, M. P.; Harvey, S. P.; Johnston, S.; Schelhas, L. T.; Larson, B. W.; Warren, E. L.; Beard, M. C.; Berry, J. J.; Yan, Y.; Zhu, K. Compositional texture engineering for highly stable wide-bandgap perovskite solar cells. *Science* **2022**, *378* (6626), 1295−1300.

(3) Sidhik, S.; Wang, Y.; De Siena, M.; Asadpour, R.; Torma, A. J.; Terlier, T.; Ho, K.; Li, W.; Puthirath, A. B.; Shuai, X.; Agrawal, A.; Traore, B.; Jones, M.; Giridharagopal, R.; Ajayan, P. M.; Strzalka, J.; Ginger, D. S.; Katan, C.; Alam, M. A.; Even, J.; Kanatzidis, M. G.; Mohite, A. D. Deterministic fabrication of 3D/2D perovskite bilayer stacks for durable and efficient solar cells. *Science* **2022**, *377* (6613), 1425−1430.

(4) Li, W.; Sidhik, S.; Traore, B.; Asadpour, R.; Hou, J.; Zhang, H.; Fehr, A.; Essman, J.; Wang, Y.; Hoffman, J. M.; Spanopoulos, I.; Crochet, J. J.; Tsai, E.; Strzalka, J.; Katan, C.; Alam, M. A.; Kanatzidis, M. G.; Even, J.; Blancon, J.-C.; Mohite, A. D. Light-activated interlayer contraction in two-dimensional perovskites for high-efficiency solar cells. *Nat. Nanotechnol.* **2022**, *17* (1), 45−52.

(5) Tsai, H.; Nie, W.; Blancon, J.-C.; Stoumpos, C. C.; Asadpour, R.; Harutyunyan, B.; Neukirch, A. J.; Verduzco, R.; Crochet, J. J.; Tretiak, S.; Pedesseau, L.; Even, J.; Alam, M. A.; Gupta, G.; Lou, J.; Ajayan, P. M.; Bedzyk, M. J.; Kanatzidis, M. G.; Mohite, A. D. High-efficiency two-dimensional Ruddlesden-Popper perovskite solar cells. *Nature* **2016**, *536* (7616), 312−316.

(6) Mitzi, D. B.; Chondroudis, K.; Kagan, C. R. Organic-inorganic electronics. *IBM J. Res. Dev.* **2001**, *45* (1), 29−45.

(7) Katan, C.; Mercier, N.; Even, J. Quantum and Dielectric Confinement Effects in Lower-Dimensional Hybrid Perovskite Semiconductors. *Chem. Rev.* **2019**, *119* (5), 3140−3192.

(8) Almora, O.; Baran, D.; Bazan, G. C.; Berger, C.; Cabrera, C. I.; Catchpole, K. R.; Erten-Ela, S.; Guo, F.; Hauch, J.; Ho-Baillie, A. W. Y.; Jacobsson, T. J.; Janssen, R. A. J.; Kirchartz, T.; Kopidakis, N.; Li, Y.; Loi, M. A.; Lunt, R. R.; Mathew, X.; McGehee, M. D.; Min, J.; Mitzi, D. B.; Nazeeruddin, M. K.; Nelson, J.; Nogueira, A. F.; Paetzold, U. W.; Park, N.-G.; Rand, B. P.; Rau, U.; Snaith, H. J.; Unger, E.; Vaillant-Roca, L.; Yip, H.-L.; Brabec, C. J. Device Performance of Emerging Photovoltaic Materials (Version 1). *Adv. Energy Mater.* **2021**, *11* (11), 2002774.

(9) García de Arquer, F. P.; Armin, A.; Meredith, P.; Sargent, E. H. Solution-processed semiconductors for next-generation photodetectors. *Nat. Rev. Mater.* **2017**, *2* (3), 16100.

(10) Li, G.; Wang, Y.; Huang, L.; Sun, W. Research Progress of High-Sensitivity Perovskite Photodetectors: A Review of Photodetectors: Noise, Structure, and Materials. *ACS Appl. Electron. Mater.* **2022**, *4* (4), 1485−1505.

(11) Dohner, E. R.; Hoke, E. T.; Karunadasa, H. I. Self-assembly of broadband white-light emitters. *J. Am. Chem. Soc.* **2014**, *136* (5), 1718−1721.

(12) Zhang, L.; Sun, C.; He, T.; Jiang, Y.; Wei, J.; Huang, Y.; Yuan, M. High-performance quasi-2D perovskite light-emitting diodes: from materials to devices. *Light: Sci. Appl.* **2021**, *10* (1), 61.

(13) Qin, C.; Sandanayaka, A. S. D.; Zhao, C.; Matsushima, T.; Zhang, D.; Fujihara, T.; Adachi, C. Stable room-temperature continuous-wave lasing in quasi-2D perovskite films. *Nature* **2020**, *585* (7823), 53−57.

(14) Kagan, C. R.; Mitzi, D. B.; Dimitrakopoulos, C. D. Organic-Inorganic Hybrid Materials as Semiconducting Channels in Thin-Film Field-Effect Transistors. *Science* **1999**, *286* (5441), 945−947.

(15) Chen, P.; Bai, Y.; Wang, S.; Lyu, M.; Yun, J.-H.; Wang, L. In Situ Growth of 2D Perovskite Capping Layer for Stable and Efficient Perovskite Solar Cells. *Adv. Funct. Mater.* **2018**, *28* (17), 1706923.

(16) Yan, J.; Li, H.; Aldamasy, M. H.; Frasca, C.; Abate, A.; Zhao, K.; Hu, Y. Advances in the Synthesis of Halide Perovskite Single Crystals for Optoelectronic Applications. *Chem. Mater.* **2023**, *35* (7), 2683−2712.

(17) Li, H.; Shen, N.; Chen, S.; Guo, F.; Xu, B. Recent Progress on Synthesis, Intrinsic Properties and Optoelectronic Applications of Perovskite Single Crystals. *Adv. Funct. Mater.* **2023**, *33* (24), 2214339.

(18) Billing, D. G.; Lemmerer, A. Synthesis, characterization and phase transitions in the inorganic-organic layered perovskite-type hybrids $[(C_nH_{2n+1}NH_3)_2PbI_4]$, n = 4, 5 and 6. *Acta Crystallogr., Sect. B: Struct. Sci.* **2007**, *63* (Pt 5), 735−747.

(19) Lemmerer, A.; Billing, D. G. Synthesis, characterization and phase transitions of the inorganic-organic layered perovskite-type hybrids $[(C_nH_{2n+1}NH_3)_2PbI_4]$, n = 7 8, 9 and 10. *Dalton Trans.* **2012**, *41* (4), 1146−1157.

(20) Billing, D. G.; Lemmerer, A. Synthesis, characterization and phase transitions of the inorganic-organic layered perovskite-type hybrids $[(C_nH_{2n+1}NH_3)_2PbI_4]$ (n = 12, 14, 16 and 18). *New J. Chem.* **2008**, *32* (10), 1736−1746.

(21) Van Gompel, W. T. M.; Lutsen, L.; Vanderzande, D. 2D and quasi-2D hybrid perovskites containing organic cations with an extended conjugated system: opportunities and challenges. *J. Mater. Chem. C* **2023**, *11*, 12877−12893.

(22) Herckens, R.; Van Gompel, W. T. M.; Song, W.; Gélvez-Rueda, M. C.; Maufort, A.; Ruttens, B.; D'Haen, J.; Grozema, F. C.; Aernouts, T.; Lutsen, L.; Vanderzande, D. Multi-layered hybrid perovskites templated with carbazole derivatives: optical properties, enhanced moisture stability and solar cell characteristics. *J. Mater. Chem. A* **2018**, *6* (45), 22899−22908.

(23) Boeije, Y.; Van Gompel, W. T. M.; Zhang, Y.; Ghosh, P.; Zelewski, S. J.; Maufort, A.; Roose, B.; Ooi, Z. Y.; Chowdhury, R.; Devroey, I.; Lenaers, S.; Tew, A.; Dai, L.; Dey, K.; Salway, H.; Friend, R. H.; Sirringhaus, H.; Lutsen, L.; Vanderzande, D.; Rao, A.; Stranks, S. D. Tailoring Interlayer Charge Transfer Dynamics in 2D Perovskites with Electroactive Spacer Molecules. *J. Am. Chem. Soc.* **2023**, *145* (39), 21330−21343.

(24) Van Landeghem, M.; Van Gompel, W.; Herckens, R.; Lutsen, L.; Vanderzande, D.; Van Doorslaer, S.; Goovaerts, E. Light-Induced Charge Transfer in Two-Dimensional Hybrid Lead Halide Perovskites. *J. Phys. Chem. C* **2021**, *125* (33), 18317−18327.

(25) Lammar, S.; Van Gompel, W.; Lenaers, S.; Mertens, M.; Boyen, H.-G.; Desta, D.; Hadipour, A.; Lutsen, L.; Vanderzande, D.; Krishna, A.; Abdulraheem, Y.; Aernouts, T.; Poortmans, J. Organic ammonium iodide salts as passivation for buried interface enables efficient and stable NiO_x based p-i-n perovskite solar cells. *J. Mater. Chem. C* **2023**, *11* (24), 8146−8153.

(26) Passarelli, J. V.; Fairfield, D. J.; Sather, N. A.; Hendricks, M. P.; Sai, H.; Stern, C. L.; Stupp, S. I. Enhanced Out-of-Plane Conductivity and Photovoltaic Performance in n = 1 Layered Perovskites through Organic Cation Design. *J. Am. Chem. Soc.* **2018**, *140* (23), 7313−7323.

(27) Gao, Y.; Wei, Z.; Yoo, P.; Shi, E.; Zeller, M.; Zhu, C.; Liao, P.; Dou, L. Highly Stable Lead-Free Perovskite Field-Effect Transistors Incorporating Linear pi-Conjugated Organic Ligands. *J. Am. Chem. Soc.* **2019**, *141* (39), 15577−15585.

(28) Liang, A.; Gao, Y.; Asadpour, R.; Wei, Z.; Finkenauer, B. P.; Jin, L.; Yang, J.; Wang, K.; Chen, K.; Liao, P.; Zhu, C.; Huang, L.; Boudouris, B. W.; Alam, M. A.; Dou, L. Ligand-Driven Grain Engineering of High Mobility Two-Dimensional Perovskite Thin-Film Transistors. *J. Am. Chem. Soc.* **2021**, *143* (37), 15215−15223.

(29) Zhang, X.; Eurelings, S.; Bracesco, A.; Song, W.; Lenaers, S.; Van Gompel, W.; Krishna, A.; Aernouts, T.; Lutsen, L.; Vanderzande, D.; Creatore, M.; Zhan, Y.; Kuang, Y.; Poortmans, J. Surface Modulation via Conjugated Bithiophene Ammonium Salt for Efficient Inverted Perovskite Solar Cells. *ACS Appl. Mater. Interfaces* **2023**, *15*, 46803−46811.

(30) Denis, P.-H.; Mertens, M.; Van Gompel, W. T. M.; Maufort, A.; Mertens, S.; Wei, Z.; Van Landeghem, M.; Gielen, S.; Ruttens, B.; Deduytsche, D.; Detavernier, C.; Lutsen, L.; Grozema, F.; Vandewal, K.; Vanderzande, D. Quasi-2D Hybrid Perovskite Formation Using Benzothieno[3,2-b]Benzothiophene (BTBT) Ammonium Cations: Substantial Cesium Lead(II) Iodide Black Phase Stabilization. *Adv. Opt. Mater.* **2022**, *10* (18), 2200788.

(31) Gélvez-Rueda, M. C.; Van Gompel, W. T. M.; Herckens, R.; Lutsen, L.; Vanderzande, D.; Grozema, F. C. Inducing Charge Separation in Solid-State Two-Dimensional Hybrid Perovskites through the Incorporation of Organic Charge-Transfer Complexes. *J. Phys. Chem. Lett.* **2020**, *11* (3), 824−830.

(32) Van Gompel, W. T. M.; Herckens, R.; Van Hecke, K.; Ruttens, B.; D'Haen, J.; Lutsen, L.; Vanderzande, D. Towards 2D layered hybrid perovskites with enhanced functionality: introducing charge-transfer complexes via self-assembly. *Chem. Commun.* **2019**, *55* (17), 2481−2484.

(33) Marchal, N.; Van Gompel, W.; Gélvez-Rueda, M. C.; Vandewal, K.; Van Hecke, K.; Boyen, H.-G.; Conings, B.; Herckens, R.; Maheshwari, S.; Lutsen, L.; Quarti, C.; Grozema, F. C.; Vanderzande, D.; Beljonne, D. Lead-Halide Perovskites Meet Donor-Acceptor Charge-Transfer Complexes. *Chem. Mater.* **2019**, *31* (17), 6880−6888.

(34) Passarelli, J. V.; Mauck, C. M.; Winslow, S. W.; Perkinson, C. F.; Bard, J. C.; Sai, H.; Williams, K. W.; Narayanan, A.; Fairfield, D. J.; Hendricks, M. P.; Tisdale, W. A.; Stupp, S. I. Tunable exciton binding energy in 2D hybrid layered perovskites through donor-acceptor interactions within the organic layer. *Nat. Chem.* **2020**, *12* (8), 672−682.

(35) Caiazzo, A.; Maufort, A.; van Gorkom, B. T.; Remmerswaal, W. H. M.; Orri, J. F.; Li, J.; Wang, J.; van Gompel, W. T. M.; Van Hecke, K.; Kusch, G.; Oliver, R. A.; Ducati, C.; Lutsen, L.; Wienk, M. M.; Stranks, S. D.; Vanderzande, D.; Janssen, R. A. J. 3D Perovskite Passivation with a Benzotriazole-Based 2D Interlayer for High-Efficiency Solar Cells. *ACS Appl. Energy Mater.* **2023**, *6* (7), 3933−3943.

(36) Fateev, S. A.; Petrov, A. A.; Ordinartsev, A. A.; Grishko, A. Y.; Goodilin, E. A.; Tarasov, A. B. Universal Strategy of 3D and 2D Hybrid Perovskites Single Crystal Growth via In Situ Solvent Conversion. *Chem. Mater.* **2020**, *32* (22), 9805−9812.

(37) Du, K. Z.; Tu, Q.; Zhang, X.; Han, Q.; Liu, J.; Zauscher, S.; Mitzi, D. B. Two-Dimensional Lead(II) Halide-Based Hybrid Perovskites Templated by Acene Alkylamines: Crystal Structures, Optical Properties, and Piezoelectricity. *Inorg. Chem.* **2017**, *56* (15), 9291−9302.

(38) Denis, P.-H.; Mertens, M.; Van Gompel, W. T. M.; Van Hecke, K.; Ruttens, B.; D'Haen, J.; Lutsen, L.; Vanderzande, D. Directing the Self-Assembly of Conjugated Organic Ammonium Cations in Low-Dimensional Perovskites by Halide Substitution. *Chem. Mater.* **2021**, *33* (13), 5177−5188.

(39) Smith, M. D.; Jaffe, A.; Dohner, E. R.; Lindenberg, A. M.; Karunadasa, H. I. Structural origins of broadband emission from layered Pb-Br hybrid perovskites. *Chem. Sci.* **2017**, *8* (6), 4497−4504.

(40) Lemmerer, A.; Billing, D. G. Lead halide inorganic-organic hybrids incorporating diammonium cations. *CrystEngComm* **2012**, *14* (6), 1954−1966.

(41) Quarti, C.; Marchal, N.; Beljonne, D. Tuning the Optoelectronic Properties of Two-Dimensional Hybrid Perovskite Semiconductors with Alkyl Chain Spacers. *J. Phys. Chem. Lett.* **2018**, *9* (12), 3416−3424.

(42) Van Gompel, W. T. M.; Herckens, R.; Van Hecke, K.; Ruttens, B.; D'Haen, J.; Lutsen, L.; Vanderzande, D. Low-Dimensional Hybrid Perovskites Containing an Organic Cation with an Extended Conjugated System: Tuning the Excitonic Absorption Features. *ChemNanoMat* **2019**, *5* (3), 323−327.

(43) Gao, Y.; Shi, E.; Deng, S.; Shiring, S. B.; Snaider, J. M.; Liang, C.; Yuan, B.; Song, R.; Janke, S. M.; Liebman-Pelaez, A.; Yoo, P.; Zeller, M.; Boudouris, B. W.; Liao, P.; Zhu, C.; Blum, V.; Yu, Y.; Savoie, B. M.; Huang, L.; Dou, L. Molecular engineering of organic-inorganic hybrid perovskites quantum wells. *Nat. Chem.* **2019**, *11*, 1151−1157.

(44) Lédée, F.; Audebert, P.; Trippé-Allard, G.; Galmiche, L.; Garrot, D.; Marrot, J.; Lauret, J.-S.; Deleporte, E.; Katan, C.; Even, J.; Quarti, C. Tetrazine molecules as an efficient electronic diversion channel in 2D organic-inorganic perovskites. *Mater. Horiz.* **2021**, *8* (5), 1547−1560.

(45) Marchenko, E. I.; Fateev, S. A.; Petrov, A. A.; Korolev, V. V.; Mitrofanov, A.; Petrov, A. V.; Goodilin, E. A.; Tarasov, A. B. Database of Two-Dimensional Hybrid Perovskite Materials: Open-Access Collection of Crystal Structures, Band Gaps, and Atomic Partial Charges Predicted by Machine Learning. *Chem. Mater.* **2020**, *32* (17), 7383−7388.

(46) Sourisseau, S.; Louvain, N.; Bi, W.; Mercier, N.; Rondeau, D.; Boucher, F.; Buzaré, J. Y.; Legein, C. Reduced Band Gap Hybrid Perovskites Resulting from Combined Hydrogen and Halogen Bonding at the Organic-Inorganic Interface. *Chem. Mater.* **2007**, *19* (3), 600−607.

(47) Luo, B.; Guo, Y.; Xiao, Y.; Lian, X.; Tan, T.; Liang, D.; Li, X.; Huang, X. Fluorinated Spacers Regulate the Emission and Bandgap of Two-Dimensional Single-Layered Lead Bromide Perovskites by Hydrogen Bonding. *J. Phys. Chem. Lett.* **2019**, *10* (17), 5271−5276.

(48) Lemmerer, A.; Billing, D. G. Effect of heteroatoms in the inorganic-organic layered perovskite-type hybrids [(ZCnH2nNH3)-2PbI4], n = 2, 3, 4, 5, 6; Z = OH, Br and I; and

[(H3NC2H4S2C2H4NH3)PbI4]. *CrystEngComm* **2010**, *12* (4), 1290−1301.

(49) Frey, P. A. Low Barrier Hydrogen Bonds. In *Encyclopedia of Biological Chemistry*; Lennarz, W. J., Lane, M. D., Eds.; Elsevier: New York, 2004, pp 594−598.

(50) Gómez, P.; Cerdá, J.; Más-Montoya, M.; Georgakopoulos, S.; da Silva, I.; García, A.; Ortí, E.; Aragó, J.; Curiel, D. Effect of molecular geometry and extended conjugation on the performance of hydrogen-bonded semiconductors in organic thin-film field-effect transistors. *J. Mater. Chem. C* **2021**, *9* (33), 10819−10829.

(51) Dorca, Y.; Sánchez-Naya, R.; Cerdá, J.; Calbo, J.; Aragó, J.; Gómez, R.; Ortí, E.; Sánchez, L. Impact of Molecular Size and Shape on the Supramolecular Co-Assembly of Chiral Tricarboxamides: A Comparative Study. *Chem. −Eur. J.* **2020**, *26* (64), 14700−14707.

(52) Kepenekian, M.; Traore, B.; Blancon, J.-C.; Pedesseau, L.; Tsai, H.; Nie, W.; Stoumpos, C. C.; Kanatzidis, M. G.; Even, J.; Mohite, A. D.; Tretiak, S.; Katan, C. Concept of Lattice Mismatch and Emergence of Surface States in Two-dimensional Hybrid Perovskite Quantum Wells. *Nano Lett.* **2018**, *18* (9), 5603−5609.

(53) Sato, T.; Takagi, S.; Deledda, S.; Hauback, B. C.; Orimo, S.-i. Extending the applicability of the Goldschmidt tolerance factor to arbitrary ionic compounds. *Sci. Rep.* **2016**, *6* (1), 23592.

(54) Berland, K.; Cooper, V. R.; Lee, K.; Schröder, E.; Thonhauser, T.; Hyldgaard, P.; Lundqvist, B. I. van der Waals forces in density functional theory: a review of the vdW-DF method. *Rep. Prog. Phys.* **2015**, *78* (6), 066501.

(55) Thonhauser, T.; Zuluaga, S.; Arter, C. A.; Berland, K.; Schröder, E.; Hyldgaard, P. Spin Signature of Nonlocal Correlation Binding in Metal-Organic Frameworks. *Phys. Rev. Lett.* **2015**, *115* (13), 136402.

(56) Mosconi, E.; Alothman, A. A.; Long, R.; Kaiser, W.; De Angelis, F. Intermolecular Interactions of A-Site Cations Modulate Stability of 2D Metal Halide Perovskites. *ACS Energy Lett.* **2023**, *8* (1), 748−752.

(57) Nagy, P. I. Competing intramolecular vs. intermolecular hydrogen bonds in solution. *Int. J. Mol. Sci.* **2014**, *15* (11), 19562−19633.

(58) Silverman, R. B.; Holladay, M. W. Chapter 3 - Receptors. In *The Organic Chemistry of Drug Design and Drug Action (Third ed.)*; Silverman, R. B., Holladay, M. W., Eds.; Academic Press: Boston, 2014, pp 123−163.

(59) Pedesseau, L.; Sapori, D.; Traore, B.; Robles, R.; Fang, H.-H.; Loi, M. A.; Tsai, H.; Nie, W.; Blancon, J.-C.; Neukirch, A.; Tretiak, S.; Mohite, A. D.; Katan, C.; Even, J.; Kepenekian, M. Advances and Promises of Layered Halide Hybrid Perovskite Semiconductors. *ACS Nano* **2016**, *10* (11), 9776−9786.

(60) Brammer, L.; Bruton, E. A.; Sherwood, P. Understanding the Behavior of Halogens as Hydrogen Bond Acceptors. *Cryst. Growth Des.* **2001**, *1* (4), 277−290.